# ChemComm

Accepted Manuscript


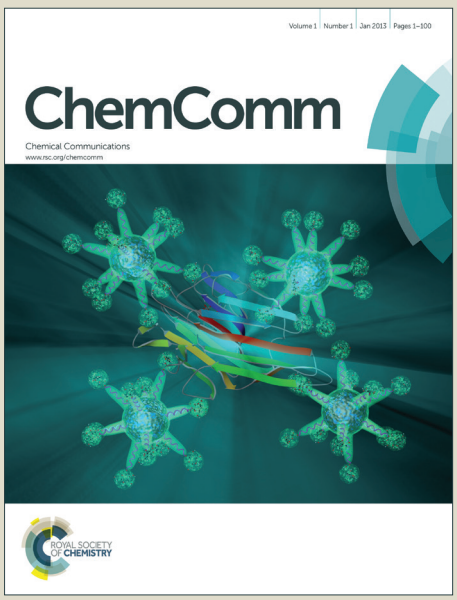





ROYAL SOCIETY OF CHEMISTRY

www.rsc.org/chemcomm

Cite this: DOI: 10.1039/c0xx00000x

www.rsc.org/xxxxxx

ARTICLE TYPE

# Remarkable Activity and Stability of Photocatalytic Hydrogen Production over Dye-Sensitized Single Molecular Layer $MoS_2$ Ensemble

Tiantian Jia, Molly M. J. Li, Lin Ye, Sam Wiseman, Guoliang Liu, Jin Qu, Keizo Nakagawa, S.C. Edman Tsang*

***Received (in XXX, XXX) Xth XXXXXXXXX 20XX, Accepted Xth XXXXXXXXX 20XX***
**DOI: 10.1039/b000000x**

**Single layer $MoS_2$ synthesized by exfoliation with Li is demonstrated to take up dye molecule, Eosin Y with a strong binding affinity via sulfur vacancy. This dye-sensitized single layer $MoS_2$ ensemble exhibits remarkable activity and stability for photocatalytic hydrogen production from water.**

*L*ayered transition metal dichalcogenides (LTMDs) attracts intensive research due to their unique electronic, optical, mechanical, and electrochemical properties, which are important for sensing, catalysis, and energy storage, etc[1-3]. Molybdenum disulfide ($MoS_2$), a widely known LTMD, is the material of research focus, which is currently used as a solid state lubricant and hydro-desulfurization catalyst in industry[4]. It is considered to be as an alternative catalyst to platinum for electrochemical generation of hydrogen from water[5-9]. Previous studies have concluded that the catalytic and electrochemical activity are linked to the active sites located along the edges with both exposure of Mo and S entities (offering active sites for low activation barrier for $H_2$ formation), while the basal plane of triangular pyramidal $MoS_2$ units covering with the compact S atoms remains to be inert[6,10]. Small $MoS_2$ nanocrystals grown on graphite[11], Au[12], carbon paper[13], carbon nanotubes[14] and graphene[15] have been showed to give excellent performances for electrocatalytic hydrogen evolution reaction (HER). While HER by electrochemical mean has been studied in detail, photocatalytic HER by $MoS_2$ has received much less attention. This is partly due to the fact that bulk $MoS_2$ is an indirect band gap semiconductor with poor photocatalytic efficiency[1,16]. In addition, the excited electrons involved for the reduction of $H^+$ to form $H_2$ cannot be photo-catalytically generated from bulk $MoS_2$ due to its characteristic lower conduction band edge energy, but can be transferred from photon capture systems such as $Ru(bpy)_3^{2+}$, Eosin Y, and CdS, respectively at higher band energies. As a result, colloidal $MoS_2$ nanoparticles with diameters of less than 10 nm was reported to demonstrate high efficiency in catalyzing HER when blended with photon capture $Ru(bpy)_3^{2+}$ systems under visible light[16]. Min and Lu[17] also reported that a thin layered $MoS_2$ grown on graphene was active for photocatalytic HER at 460 nm when combined with the dye molecule, Eosin Y (EY). We earlier reported the high activity of thin $MoS_2$ slabs on graphene in the presence of CdS nanoparticles which acted as a light absorber[18]. The recent breakthroughs in isolating single molecular layer $MoS_2$ (S-$MoS_2$) by exfoliation via Li intercalation associated with a structural change (2H-to-1T) have offered excitements to alter the 'intrinsic properties' of the layered materials[19,20]. Evidence shows that an indirect-to-direct band transition resulting in significant enhancement in photoluminescence quantum yield[13]. The band energies of $MoS_2$ can also be altered by changing the number of layers due to quantum confinement[21-23].

In this work, we report that the single molecular layer $MoS_2$ (S-$MoS_2$) and its mixture with graphene (S-$MoS_2$/graphene) can display quantifiable activity for direct photocatalytic hydrogen production from water due to the quantum confinement effect, whereas there is absolutely no hydrogen activity using thin or bulk $MoS_2$. More importantly, a dye sensitized molecule, Eosin Y containing C-Br bonds is found to readily dissociative adsorb on S-$MoS_2$ due to the presence of sulfur vacancies on the basal plane. Thus, the novel EY/S-$MoS_2$ single layer ensemble facilitates a direct electron transfer from excited EY to its bonded S-$MoS_2$, leading to efficient exciton separation for photo-catalytic decomposition of water.

$MoS_2$ was exfoliated into single layers by intercalation with lithium[24]. The starting material used in the reported studies was bulk $MoS_2$ powder from Sigma Aldrich. 500 mg of the black $MoS_2$ powder was first soaked in 8 mL of 1.6 M n-butyl lithium in hexane for 48 hours under nitrogen atmosphere. Following the intercalation of the $MoS_2$ by lithium, the produced $Li_xMoS_2$ was washed repeatedly with hexane to remove the excess butyl-lithium and dried under nitrogen atmosphere. Then the powder was immersed in water and the suspension was ultrasonicated during the reaction to assist in the exfoliation. It was assumed that the reaction between the water and the intercalated lithium forms hydrogen gas between the layers, and the expansion of this gas tends to separate the $MoS_2$ layers. As the reaction proceeded more deeply into each crystallite, the layers became further separated. Eventually the layers became completely separated and remain suspended in the aqueous solution. The pH of this solution was basic due to the presence of lithium hydroxide. See electronic supporting Information (ESI) for details on synthesis of other materials, photocatalytic activity testing and characterisation techniques.

Transmission electron microscopy (TEM) examination (Fig. S1) showed a large quantity of thin 2D flakes. A majority of the exfoliated $MoS_2$ sheets were found to be 20-60 nm but more than 100nm fake can also be observed in lateral dimensions. They mainly consisted of 1-3 layers by counting the edges. The zoom-in HRTEM in Fig S1 shows the co-existence of 1-T phase (trigonal lattice area in octahedral pattern, see Fig. 1), besides the common honey-comb lattice of the trigonal prismatic

coordination in the 2H phase[19,20]. X-ray powder diffraction and Raman spectroscopy characterization of this sample (Fig. S2 and S3) also suggest the sample contains single layer of 1T $MoS_2$[25]. Fig. 1 presents the atomic force microscopy (AFM) and scanning transmission electron microscopy (STEM) images of the S-$MoS_2$ sample supported with a structural drawing of the 1-T phase. As seen from AFM image in Fig. 1, the lateral dimension of this well dispersed S-$MoS_2$ nanosheet prepared by a high power spin coating is approximately 20-40 nm with occasionally larger size fakes observed. For the TEM (Fig. S1) we used conventional technique to disperse the sample in solvent prior dropping the dispersed sample on a copper grid holder, thus there was a significant aggregation in the sample, giving a larger fake size. . Notice that there are large amounts of single molecular layers of $MoS_2$ that can be found in the exfoliated samples. It can be seen that the step heights of individual layers of 0.6-0.7 nm in the AFM image. This value is comparable to ca. 0.65 nm of a single layer of the S-Mo-S building block[26]. Statistical analysis of 100 flakes revealed 56% of them to be monolayer, 28% two layers and 13% three layers and so on. The photocatalytic hydrogen production activities on bulk $MoS_2$ and reduced thin multilayer M-$MoS_2$ were compared to S-$MoS_2$ with or without graphene as photocatalysts under 500 W UV lamp irradiation using TEOA as a hole scavenger (Fig. 2). We can see that from the figure that there is no $H_2$ produced at all using bulk $MoS_2$ and M-$MoS_2$, which means that multi-layers of $MoS_2$ are inert for the photocatalytic hydrogen evolution reaction from water. However, the exfoliated S-$MoS_2$, clearly shows that 6.59 µL $H_2$ can be produced within one hour of irradiation. It is noted, in bulk $MoS_2$ although the accepted valence band edge potential of ca. 1.40 V can be used to oxidize $H_2O$ to $O_2$ (1.23 V), the conduction band edge of 0.25 V[27,28] is unable to reduce $H^+$ to $H_2$.. In contrast, S-$MoS_2$ gives literally lower band edge potential of -0.12 V due to quantum confinements which can thus reduce $H^+$ to $H_2$ upon photoexcitation[20,27,28]. The observation confirms the interesting properties of S-$MoS_2$ as a photocatalyst.

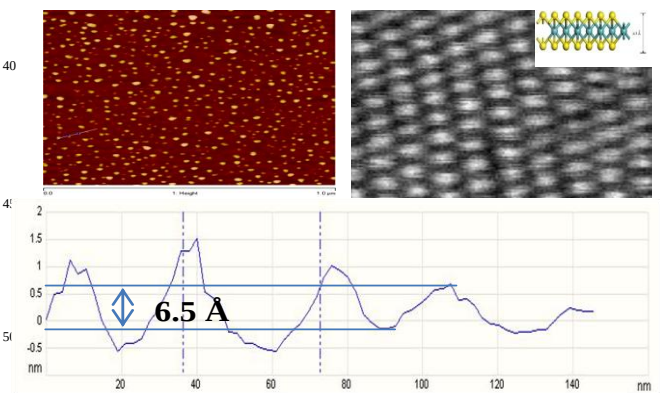


***Figure 1.*** Atomic force microscopy (AFM) image of spin coated S-$MoS_2$ onto a surface of $Si/SiO_2$ substrate. (upper left) and HAADF STEM image of 1T region of $MoS_2$ with a drawing (upper right) showing the characteristic pattern created due to Mo atoms sandwiched in the upper and lower S atom planes off-set at 30° in octahedral coordination (~3Å between bright spots), 100 flakes is scanned by AFM with majority of heights between 0.6-0.7nm (lower).

It is however, we see two technical huddles in using S-$MoS_2$ as an efficient photo-catalyst for hydrogen production, namely the intrinsic instability of S-$MoS_2$ against stacking and the low band gap (ca. 1.9 eV) & inefficient capture of visible light. First, when we studied the effect of increasing amount of S-$MoS_2$ on $H_2$ evolution rate (Fig. S4), the photocatalytic activity was found to increase from 3.34 µL/h to 11.09 µL/h at increasing concentration of S-$MoS_2$ from 0.25 mL to 10 mL (concentration= 2mg/mL) and reached the maximum $H_2$ production rate at 10 mL of S-$MoS_2$ (total volume is kept at 100mL). But at further increasing amount of S-$MoS_2$, it led to a reduction of activity due to restacking at higher concentration. This re-stacking of S-$MoS_2$ is quick and with a high propensity, as reflected by the post-XRD analysis (Fig. S2d). One potential solution is to use a high surface area solid support to disperse the single layers.

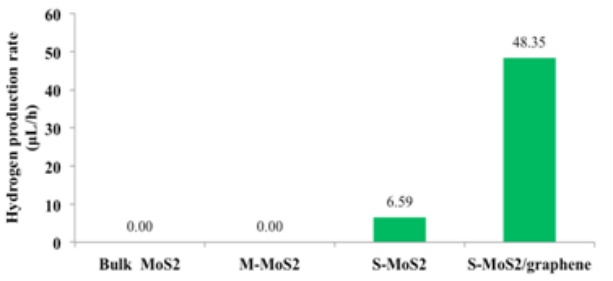


***Figure 2*** Photocatalytic hydrogen evolution from 20 mg of bulk $MoS_2$, M-$MoS_2$, S-$MoS_2$, S-$MoS_2$/graphene in 100 mL $H_2O$ with 15% (v/v) TEOA aqueous solution, under 500 W UV-Vis irradiation for one hour.

From Fig. 2, it is to note that the catalytic activity of S-$MoS_2$/graphene for $H_2$ evolution is indeed promoted to 48.35 µL/h, which is 7.3 times higher than that of pure S-$MoS_2$. TEM images of S-$MoS_2$/graphene in Fig. S1c,d clearly reveal that the $MoS_2$ sheets deposit on graphene flake, which acts as a support to reduce the extent of re-stacking (also XRD, not shown). To address the intrinsic low photon capture ability of S-$MoS_2$, we adopted the approach of solar cells by adding organic dye molecule as sensitizer[29]. A dye molecule with extensive conjugation system and also with high quantum efficiency should be selected. A high LUMO position can offer additional thermodynamic driving potential to catalyze hydrogen production via $MoS_2$. We thus tested the photocatalytic activity of samples with Eosin Y to investigate its promotion effect[17]. Fig. S5 clearly shows that the $H_2$ evolution can be dramatically catalyzed by bulk $MoS_2$, M-$MoS_2$, M-$MoS_2$/graphene, S-$MoS_2$ and S-$MoS_2$/graphene with EY as a photosensitizer in aqueous TEOA. Accordingly, the rate of $H_2$ evolution reaches to 397.02 µL/h in S-$MoS_2$ with the EY-sensitized system. The $H_2$ production rate is 1.47 times than that of M-$MoS_2$ (270.58 µL/h) and 3.24 times than bulk $MoS_2$ (122.37 µL/h). Their catalytic activity can be further enhanced to 467.53 µL/h and 340.06 µL/h, respectively when they are placed on graphene. Apart from physical dispersion of $MoS_2$, it is evident that graphene serves as conductor[18] for electrons to move from photo-excited EY* to active sites of $MoS_2$ for the hydrogen production.

It is very interesting to note a subtle difference in stability for $H_2$ production over M-$MoS_2$ and S-$MoS_2$ with or without graphene upon repeatedly testing. Fig. 3a shows that the $H_2$ evolution rate decreases significantly over M-$MoS_2$ with or without graphene with increasing reaction time. There is almost no hydrogen detected after 4 cycles. The $H_2$ evolution activity of M-$MoS_2$, M-$MoS_2$/graphene can be mostly recovered by the addition of the same quantity of EY, which implies the dye photosensitizer is progressively degraded. This degradation is commonly taken place in both solar cells and photocatalytic converter during photo-excitation but the mechanism is not fully understood. The instability of M-$MoS_2$ samples (Fig. 3b) corroborates with the attenuation and shift of the absorption bands around 500 nm, so-called photo-bleaching, which is mainly responsible for the

reductive destruction and photo-debromination of EY dye under irradiation [30,31](Fig. S6). Surprisingly, as seen from Fig. 3b, the use of S-$MoS_2$ (with slight deactivation due to re-stacking) and S-$MoS_2$/graphene are much more stable with no EY degradation (Fig. S7). Apart from the 1st testing which appears to be lower than the subsequent cycles presumably due the partial aggregation in the testing solution at the beginning of the testing. there is no significant deactivation for the S-$MoS_2$/graphene even after 10 cycles of reaction (20 hours of reaction time).

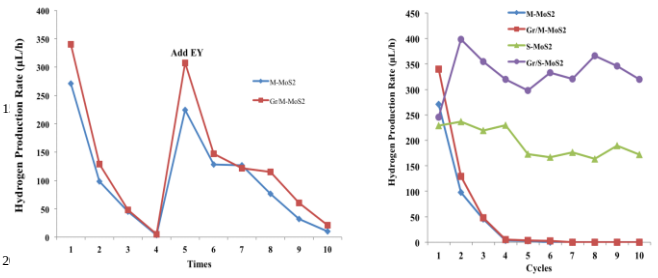


***Figure 3a*** Stability test of hydrogen evolution over EY ($4.0 \times 10^{-4}$ M) sensitized M-$MoS_2$ and M-$MoS_2$/graphene in 100 mL of 15% TEOA aqueous solution under UV irradiation evaluated every 2 hours. EY was added to the system in the fifth cycle; **3b**. Stability test of hydrogen evolution over EY ($4.0 \times 10^{-4}$M) sensitized S-$MoS_2$, S-$MoS_2$/graphene, M-$MoS_2$ and M-$MoS_2$/graphene under the same conditions without adding EY.

We believe that the difference is due to relative adsorption strength of EY with the two forms of $MoS_2$. As demonstrated by Tokumaru *et al*., free form of xanthene dyes such as EY in solution can generate one-electron reduced trianion radical species upon cathodic reduction[32], further hydrogenation of the radical, as shown in Fig. 4, can take place by disproportionation reaction between them. After the hydrogenation, the pπ-conjugated system disappears causing fading of red colour (Fig. S8). A similar photo bleaching mechanism of free EY has been noted when the dye is irradiated in TEOA without catalyst[31]. It is thus concluded that the gradual quenching of $H_2$ evolution on M-$MoS_2$-EY dye is mainly caused by the formation of hydrogenated species of weakly bound dye molecules in TEOA with M-$MoS_2$. Thus, while light source excites free or weakly bound EY to singlet state $^{1*}$EY[33], some $^{1*}$EY with no rapid electron transfer, can relax to triple state $^{3*}$EY by intersystem crossing. In the presence of TEOA, this long lived free form $^{3*}$EY species can be reductively quenched and produce the $EY^{-}\bullet$, followed by hydrogenation, leading to decolouration.

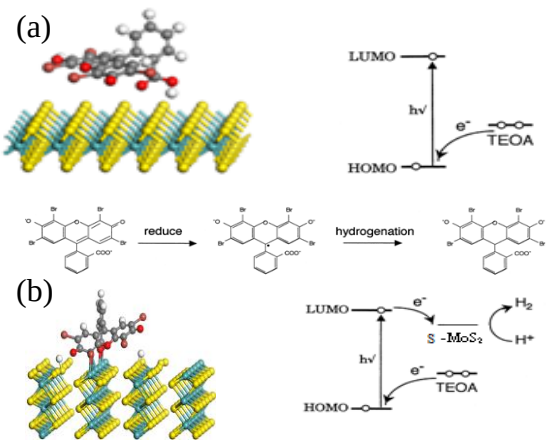


***Figure 4*** **(a)** an illustration of weak reversible adsorption of EY on complete basal planar sites of multilayer $MoS_2$ (0.06eV from DFT calculations, see ESI) hence photo-bleaching of free EY (reductive photo-destruction of dye), leading to deactivation. **(b)** An illustration of strongly chemisorbed EY on exposed Mo site (6.49eV from DFT), a rapid electron transfer from photoexcited EY to $MoS_2$ for $H_2$ production in regeneration of adsorbed EY on basal plane of single molecular layer $MoS_2$ via S vacancies to sustain activity is proposed.

In the case of S-$MoS_2$, it is envisaged that EY molecule must strongly adsorb on the S-$MoS_2$ than M-$MoS_2$ for a more rapid and efficient electron transfer from the excited $^{1*}$EY to S-$MoS_2$, which is essential for the regeneration of EY directly without its reductive degradation at longer time scale. Indeed, we observed a much larger uptake of EY molecules (more than 10 times red intensity) by S-$MoS_2$ than that of M-$MoS_2$ sample in a confocal microscopic examination after the samples were rinsed with EY solution of the same concentration, presumably due to the larger surface area of exfoliated M-$MoS_2$. It is noted from Fig. S9, EY appears to adsorb preferentially on localized edge regions of M-$MoS_2$. But for S-$MoS_2$, the florescent molecules appear to spread out more evenly for the whole layers. The S-$MoS_2$ sample was derived from the M-$MoS_2$ sample through Li intercalation and exfoliation with no significant change in the lateral size distribution. Thus the higher uptake of S-$MoS_2$ implies that the EY molecules are likely adsorbed on the newly created basal planes from exfoliation (Fig. S10). However, from our DFT calculations (Fig. 4 and SI), carboxyl group of $EY^{2-}$ could only weakly interact with surface H to form EY molecule reversibly and the calculated adsorption energy is 0.06 eV with the intact basal plane of $MoS_2$ (0001). This value would not support a strong adsorption between EY and this surface. In contrast, at $MoS_2$ $(10\bar{1}0)$, the exposed Mo on edges could give much stronger binding with the ionized carboxyl groups of $EY^{2-}$, rendering the dissociative adsorption of C-Br bond on the surface. The calculated adsorption energy is 6.49 eV. This study matches with the recent DFT modeling in literature that a strong adsorption of EY molecule on ZnO solar cell surface can take place with a direct bonding of -Br and -O (and carboxylate) terminations of the EY with exposed Lewis acid site ($Zn^{2+}$)[29]. Thus, our modeling and confocal microscopy support the fact that for the small size of M-$MoS_2$, there would be weak adsorption of EY with its predominant intact basal plane surfaces, accounting for the progressive deactivation due to photo degradation of EY primarily from free or weakly bound forms. On the other hand, it is well accepted Li transfer its electron to $MoS_2$ framework upon intercalation. This chemical synthesis is recently shown to generate a large quantity of sulfur vacancies on S-$MoS_2$ (0001), which induces significant structural (2H to 1T), electronic and magnetic changes[19,34]. Thus, the sulfur defective basal plane of our synthesized S-$MoS_2$ which can expose surface Lewis acid sites, $Mo^{4+}$ akin to the edge region for the stronger dissociative adsorption of EY molecules. Indeed, we observed a large deviation of S/Mo ratio in S-$MoS_2$ from calibrated EDX analysis (1.8 versus 2.0 in bulk $MoS_2$) and the detachment of Br atoms from EY in our mass spectroscopy analysis after its reaction over S-$MoS_2$ (Fig. S11). This may suggest a direct Lewis acid-base bonding between EY and S-$MoS_2$ as similar to the case of EY on ZnO[29] although further evidence to show the chemical linkage is required. In addition, adsorption of EY molecules could also be taken place on graphene in close proximity to the S-$MoS_2$, which could enhance their interaction[35].

To verify the importance of the rapid electron-transport mechanism in this likely covalent bonded EY-single molecular $MoS_2$ ensemble, static and time-resolved photo-luminescence (PL)

spectroscopy were employed on a film containing these ensembles. Interestingly, the static PL spectra in Fig.S5 in the ESI suggest that the high luminescence intensity at 600nm associated with singular state $^{1*}$EY is totally quenched in the presence S-$MoS_2$. Fig.5 shows the luminescence time-decay curves of EY and EY with S-$MoS_2$ ensemble in the 0.1 to 10 ns range (Fig S12 and Tables S1-S2). It is clearly evident that a decay lifetime of 0.8-1.3ns, a typical timescale of $^{1*}$EY from free and weakly bound EY is seen[36,37] (the lifetime of $^{3*}$EY is in ms[34]). However, our ps-TRPL indicates that there is indeed a significant faster electronic transfer between photo-excited but strongly bound EY to S-$MoS_2$ in this novel single layer EY-S-$MoS_2$ ensemble (~0.29 ns). Thus the direct attachment of conjugated rings of EY to Mo through chemisorption of sulfur vacancies on S-$MoS_2$ can facilitate a faster electron transfer from the excited $^{1*}$EY to active sites on S-$MoS_2$ for hydrogen production hence preventing the photodegrdation EY route via the longer lifetime of $^{3*}$EY. It is noted that Abe et al.[38] have chemically tethered the EY dye on photoactive Pt/$TiO_2$ via silane-coupling reagent. They argued that using their dye-fixed system, electron transfer can take place without the dye being hydrogenated by the TEOA or Pt. However, they observed low activity and more pronounced deactivation than this work due to poor electronic conductivity across the organo-silane and the instability of their complex interactions. The importance of fast photoactivation and electron transfer over graphitic carbon nitride support in related systems is also discussed[39,40].

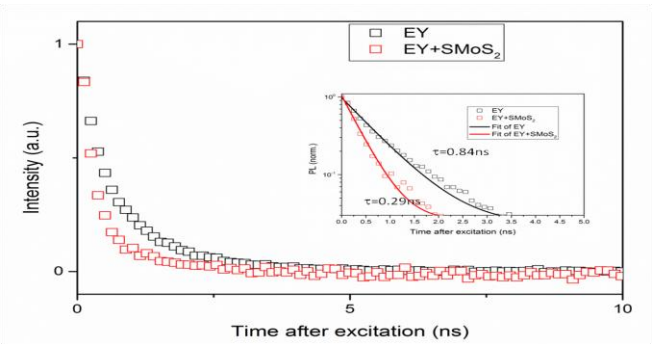


***Figure 5.*** Time-resolved Photoluminescence of Eosin Y and Eosin Y/S-$MoS_2$ on a glass slide excited using a 405 nm laser pulsed at frequencies of 32 MHZ.

In conclusion, we show the first simple methodology to modify the S-$MoS_2$ for photocatalysis by EY molecule via a strong interaction with sulfur vacancy. The EY-S-$MoS_2$-graphene ensemble shows excellent activity and stability in hydrogen evolution from water. It is attributed to the efficient caption of photons by surface bound EY molecules and faster electron transfer through the direct chemical linkage of conjugated rings of EY with exposed Lewis acidic $Mo^{4+}$ of S-$MoS_2$ on basal plane.

## Notes and references

*Department of Chemistry, University of Oxford, Oxford, OX1 3QR, UK; E-mail: edman.tsang@chem.ox.ac.uk;*

*†Electronic Supplementary Information (ESI) available: details in sample preparation, testing and characterization, see DOI:*


1. J. Zheng, H. Zhang, S. Dong, K. P. Loh, *Nature Comm.* 2014, **5**, 2995.
2. J. A. Wilson, A. D. Yoffe, *Adv. Phys.* 1969, **18**, 193.
3. K. S. Novoselov *et al*., *Nature* 2012, **490**, 192.
4. R. Prins, V. De Beer, G. A. Somorjai, *Catal. Rev. Sci. Eng.* 1989, **1**, 31.
5. B. Hinnemann *et al*., *J. Am. Chem. Soc.* 2005, **127**, 5308.
6. T. F. Jaramillo, K. P. Jørgensen, J. Bonde, J. H. Nielsen, S. Horch, I. orkendorff, Science 2007, **317**, 100.
7. Y. Li *et al*., *J. Am. Chem. Soc*. 2011, **133**, 7296.
8. X. Zong *et al*., *J. Am. Chem. Soc.* 2008, **130**, 7176.
9. D. Merki, S. Fierro, H. Vrubel, X. Hu, *Chem. Sci.* 2011, **2**, 1262.
10. B. Hinnemann, P. G. Moses, J. Bonde, K. P. Jørgensen, J. H. Nielsen, S. Horch, I. Chorkendorff, J. K. Nørskov, *J. Am. Chem. Soc.* 2005, **127**, 5308.
11. B. Hinnemann, P. G. Moses, J. Bonde, K. P. Jorgensen, J. H. Nielsen, S. Horch, I. Chorkendorff, J. K. Nørskov, *J. Am. Chem. Soc.* 2005, **127**, 5308.
12. M. A. Lukowski, A. S. Daniel, F. Meng, A. Forticaux, L. Li, S. Jin, *J. Am. Chem. Soc.* 2013, **135**, 10274.
13. J. Bonde, P. G. Moses, T. F. Jaramillo, J. K. Nørskov, I. Chorkendorff, *Faraday Discuss.* 2008,**140**, 219.
14. I. Chorkendorff, et al *Energy Environ. Sci.* 2012, **5**, 5577.
15. Y. Li, H. Wang, H. Dai. *Et al. J. Am. Chem. Soc.* 2011, **133**, 7296.
16. X. Zong, Y. Na, F. Wen, G. Ma, J. Yang, D. Wang, Y. Ma, M. Wang, L. Sun, C. Li, *Chem. Commun.* 2009, 4536.
17. S. Min, G. Lu. *J. Phys. Chem. C* 2012, **116**, 25413.
18. T. Jia, A. Kolpin, S.C. Tsang. *Chem. Comm*. 2014, **50**, 1185-1188.
19. L. Cai et al. JACS DOI:10.1021/ja5120908, 2014 and references therein
20. U. Maitra, U. Gupta, M. De, R. Datta, A. Govindaraj, C. N. R. Rao, *Angew. Chem. Int. Ed.* 2013, **52**, 13057.
21. R. A. Neville, B. L. Evans, *Phys. Status Solidi B* 1976, **73**, 597.
22. T. S. Li, G. L. Galli, *J. Phys. Chem. C* 2007, **111**, 16192.
23. J. N. Coleman *et al*. *Science* 2011, **331**, 568.
24. P. Joensen, R. F. Frindt, S. R. Morrison, *Mater.Res. Bull.* 1986, **21**, 457.
25. P. Joensen, E. D. Crozier, N. Alberding, R. F. Frindt. *J. Phys. C: Solid State Phys.* 1987, **20**, 4043.
26. B. Radisavljevic, A. Radenovic, J. Brivio, V. Giacometti, A. Kis, *Nature Nanotechnology* 2010, **6**, 147.
27. N. Singh, G. Jabbour. *et al. Eur. Phys. J. B* 2012, **85**, 392.
28. M. Chhowalla et al. *Nano Lett.* 2011, **11**, 5111.
29. F. Labat, I. Ciofini, H. P. Hratchian, M. Frisch, K. Raghavachari, C. Adamo, *J. Am. Chem. Soc.* 2009, **131**, 14290.
30. X. Liu, Y. X. Li, S. Q. Peng, G. X. Lu and S. B. Li, *Int. J. Hydrogen Energy* , 2012, **37**, 12150.
31. X. Liu, Y. X. Li, S. Q. Peng, G. X. Lu and S. B. Li, *Int. J. Hydrogen Energy*, 2013, **38**, 11709.
32. Y. Nishimura, H. Sakuragi, K. Tokumaru, *Denki Kagaku* 1994, **2**, 183.
33. J. Moser, M. Gratzal. *J. Am. Chem. Soc.* 1984, **106**, 6557.
34. M. A. Py; R. R. Haering, Can. *J. Phys.* 1983, **61**, 76.
35. W. Zhang, Y. Li, S. Peng, X. Cai, *Beilstein J. Nanotechnol.* 2014, **5**, 801.
36. V. Balzani, P. Ceroni, S. Gestermann, M. Gorka, C. Kauffmann, F. Vogtle, *Tetrahedron* 2002, **58**, 629.
37. D. F. Wilson, et al. *J. Bio. Chem.* 1987, **262**, 5476.
38. R. Abe *et al*. *J. Photochem. Photobio. A: Chem* 2000, **137**, 63.
39. J. Xu, Y. Li, S. Peng,Int J Hydrogen Energy, 2015, **40**, 353.
40. J. Xu, Y. Li, S. Peng, G. Lu, S. Li, Phys Chem Chem Phys, 2013, **15**, 7657.